JOURNAL OF MATERIALS SCIENCE **34** (1999) 395–406

Low velocity response of simple geometry pultruded glass/polyester composite

M. WISHEART, M. O. W. RICHARDSON*
Institute of Polymer Technology and Materials Engineering, Loughborough University, Loughborough, Leicestershire LE11 3TU, UK

This paper describes an investigation into the low velocity impact response of relatively simple geometry coupons taken from a pultruded glass/polyester product. The pultruded lay-up is a typical three ply design – a unidirectional fibre ply sandwiched between two continuous filament mat plies. By employing a simple geometry the impact response under transverse and longitudinal bending, and shear loading are considered. Impact tests from low energy through to final failure were conducted using the instrumented falling weight impact test technique. Through a detailed analysis involving ultrasonic C-scan, optical microscopy, and thermal deply all the major damage modes (delamination, fibre breakage and matrix cracking) were related to the force-deflection responses.

1. Introduction

Composite laminates are particularly susceptible to impact damage and dramatic strength reductions can occur even in the presence of barely visible impact damage [1–6]. In the literature there is a great deal of information regarding the impact, response of composites and much work has been performed over a wide range of velocities. Transverse impact resistance is particularly low due to the lack of through-thickness, reinforcement with interlaminar stresses – shear and tension – often the stresses which cause first failure due to the correspondingly low interlaminar strengths [7]. As a result, design failure strains of 0.5% are used to guard against impact failure, resulting in the excellent in-plane strength and stiffness properties of composites not being fully utilised. Understanding complex and varied impact damage modes, including matrix cracking, delamination and fibre breakage, and interactions between the three, remains an area of high research interest [8, 9]. The understanding of strain-rate effects for this system under impact loading is described elsewhere [10, 11].

The majority of impact testing reported in the literature has been on carbon/epoxy systems as these are the most common systems in the aerospace sector. Little work has been reported on either glass/polyester systems and less on pultruded composites. Svenson *et al.* [12] performed line impact tests on glass/polyester and glass/vinylester pultrusions in their investigation into the application of pultruded composites as roadside safety structures, however only global failure modes were reported in a three-point bend test configuration. Habib [13] performed tests on thick glass/polyester flat panels and reported low energy damage in the form of delamination and transverse cracks, whilst at higher energies surface damage and fibre fracture were observed. Further impact tests on thick glass/polyester flat panels were carried out by Zhou and Davies [14]. They described a three stage sequential damage model, with the first stage being elastic response to the initial damage threshold. The second stage was dominated by bending with reduced stiffness due to delamination, and the final stage was initiated by "shear-out" of the top plies causing extensive delamination.

Pultrusions generally involve a mixture of randomly oriented fibre layers (i.e. continuous filament mats (CFM)) and unidirectional fibre (UD) layers. Whereas most of the work reported was performed on laminates consisting of unidirectional plies with varying fibre orientation. Detailed impact response and damage modes of pultruded composites have not been reported previously in the literature, therefore the impact test programme was designed so that all the major damage modes were induced. By testing over the energy range from elastic impact to final failure, damage mode initiation, propagation, and interactions were related to the impact response, thus enabling the impact behaviour of the typical CFM/UD/CFM pultruded lay-up to be characterised.

2. Methodology

2.1. Impact testing

The tests were performed using the instrumented falling weight impact (IFWI) technique, which has been employed by many authors [15–20] to test composite materials. A Rosand Precision Impact Test Machine IFW5 was employed, with a variable mass and geometry

* Author to whom all correspondence should be addressed.

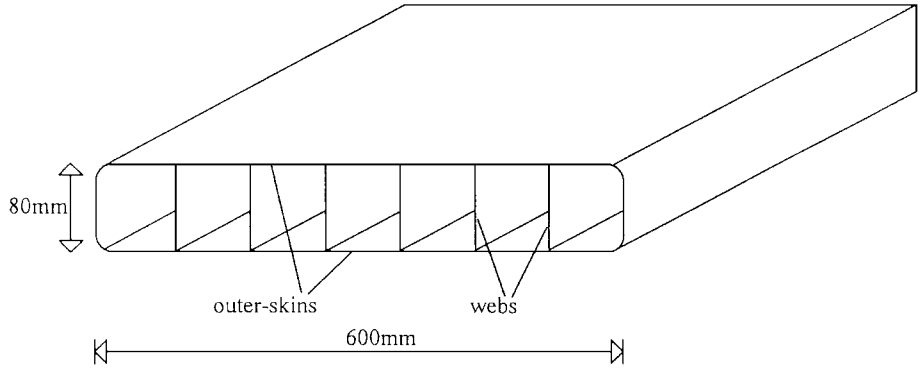

Figure 1 Simplified diagram of the pultruded section.

impactor and a second-strike prevention facility for sub-penetration energy impacts (i.e. when the impactor bounces on the specimen). An optical sensor was employed to measure the impact velocity and to trigger data capture. Filtering was not performed on these results as the unfiltered signal was relatively clear and over filtering can remove significant peaks and reduces the peak values recorded [16–18]. The impactor mass (10.8 kg) was constant throughout the tests and the impact energy altered by varying the impactor velocity (by altering the drop height) from very low energies up to final failure. At each energy approximately five tests were performed, each with a 10 mm diameter hemispherical tipped impactor.

2.2. Damage analysis

In order to assess all the damage modes, in addition to the visual inspection, optical microscopy, and ultrasonic C-scan performed by Zhou and Davies [14], thermal deply testing was also performed to assess fibre breakage. **Optical microscopy** inspection was performed on sections cut from the damaged area to provided quantitative and qualitative information on matrix cracking and delamination patterns. In order to obtain a three-dimensional map of matrix cracking and delamination, the impacted specimens were cut into transverse strips (a similar approach is described by Hong and Liu [21]) with the number of surfaces inspected maintained at approximately eight. The specimens were cut, polished with progressively finer grades of silicon carbide, and then a highlighter pen drawn across the polished surface and the excess ink removed by wiping with a clean cloth. The remaining ink highlighted the matrix cracks and delaminations. Every impact specimen was subjected to an **ultrasonic C-scan**, obtained via a 2.25 MHz alpha type transmitter employed with a Wells Krautkramer Flaw Detector USIP 12 system. The specimens chosen for **thermal deply analysis** were placed in a Eurotherm Muffle Furnace (600 °C for approximately three hours), situated in a standard fume cupboard, to burn off the resin. The technique was employed to obtain the extent of fibre breakage in the impacted specimen.

2.3. Test specimen

A coupon is a simple geometry specimen on which initial studies can be performed before a more complex structure is examined. The coupons were designed and supported so as to respond in a different primary response mode: shear, transverse bending, and longitudinal bending. By reducing the geometrical complexity to a minimum, the material behaviour in each response mode dominated thus enabling a clearer understanding of the material. The three different coupons, named the *shear coupon, longitudinal and transverse coupon* were all taken from the 3.4 mm thick outer-skin of the pultruded composite section as shown in Fig. 1. The primary material components of the section were E-glass fibres and isophthalic polyester resin. The outer skins consist of unidirectional fibres sandwiched between continuous filament mats with a polymeric veil on the outer surface to improve the appearance.

The geometry of the coupons are shown in Figs 2–4. The shear coupons were clamped between the anvil and clamp as shown in Fig. 5. The clamped supports introduced high shear forces, hence the coupon's name. The transverse coupon responded as if it was a transverse flexural test (i.e. the UD fibres were at 90° to the major plane of bending). These coupons were stiff in the longitudinal direction due to the stiffeners and UD fibres, whilst being relatively compliant in the transverse direction because the only fibres in this direction were those randomly oriented in the CFM plies. In the longitudinal coupon the unidirectional fibres were parallel with the long edge of the coupon, therefore on central impact, the specimen flexed primarily in the longitudinal direction. The impact site was central for each of the coupons.

3. Results

3.1. Shear coupon

The force-deflection curves clearly indicated a change in stiffness (at approximately 1.3 kN) during the impact event and this is referred to as the "knee" (Fig. 6). The basic shape of the curve was very similar to that reported by Zhou and Davies [14] and Jackson and Poe [22] with an initial knee followed by a less stiff response up to the peak load.

The impactor penetrated for the two highest energy impacts, with the peak force flattening off at 3.3 kN (Fig. 7). The error bars on each graph indicate that there was a good level of repeatability within each set of tests. The continuous line plotted in Fig. 7 corresponds to a modified spring-mass model prediction of the elastic

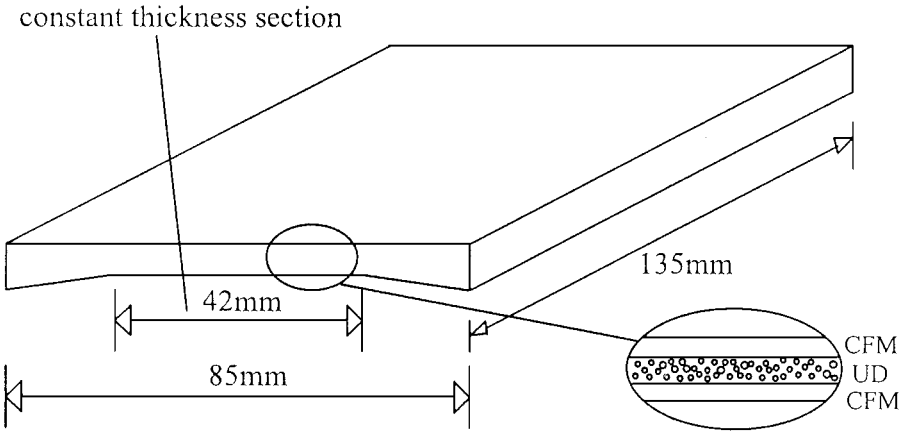

Figure 2 Shear coupon geometry.

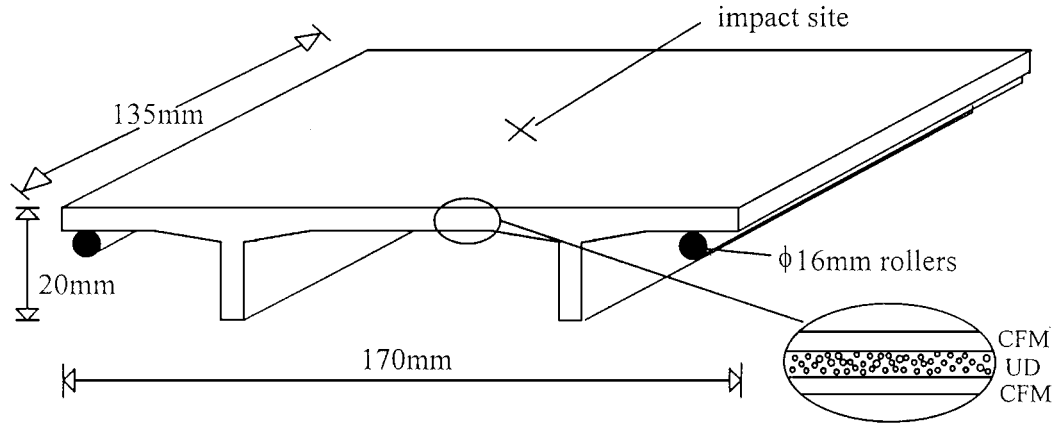

Figure 3 Transverse coupon geometry and support conditions.

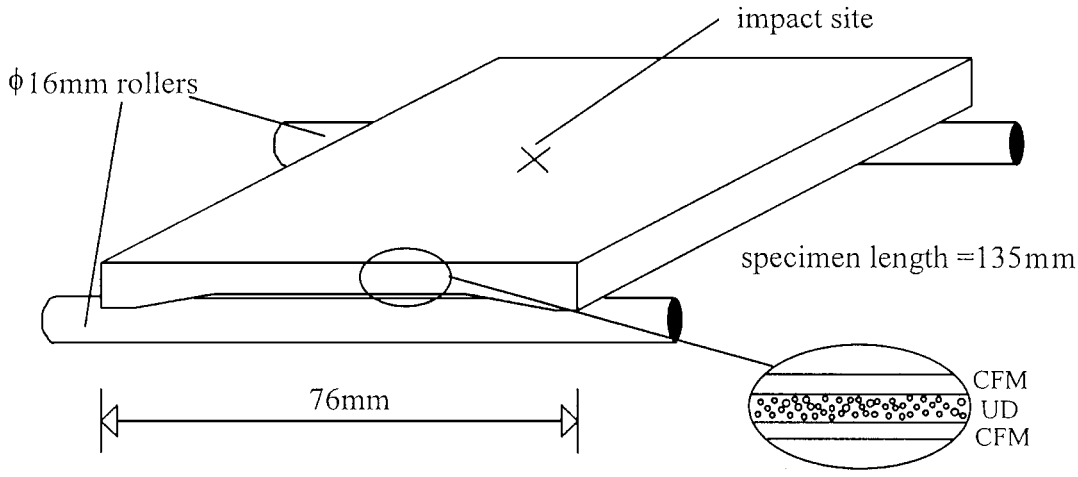

Figure 4 Longitudinal coupon geometry and support conditions.

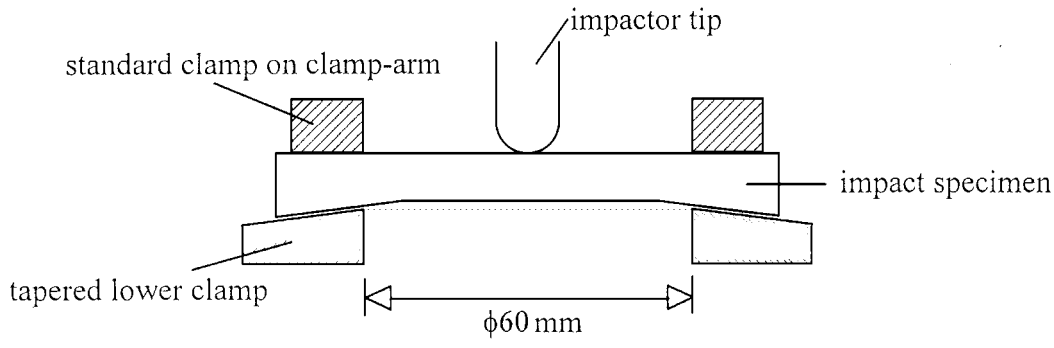

Figure 5 Clamped support conditions for the coupon impact tests.

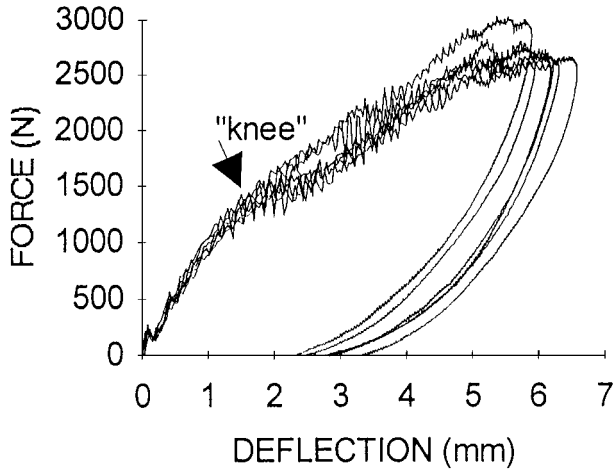

Figure 6 Force-deflection curve for the 10.9 J TIE shear coupons.

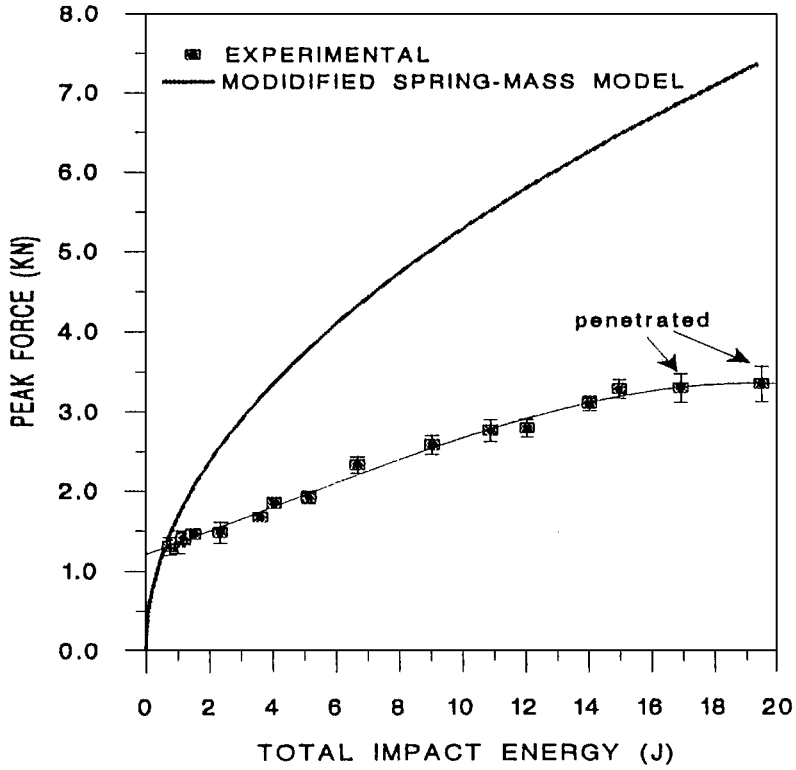

Figure 7 Peak force versus TIE for the shear coupon, and modified spring-mass model prediction.

relationship between peak force versus total impact energy (TIE). The graph clearly show that the reduction in stiffness due to damage was dramatic, and even at the lowest energy some damage was induced. The standard spring-mass model gives the following relationship between peak force and impact energy:

$$F_{\max} = \sqrt{(2U_0K)} \tag{1}$$

where $U_0 =$ impact energy (J), $K =$ spring stiffness (N/m). The "term total impact energy" is described in an earlier work by these authors [10, 11] and equals $1/2mv_0^2 + mg\delta$, ($\delta =$ max. central deflection) which corresponds to the total energy absorbed by the specimen on a rebound test. When this is inserted into Equation 1, it becomes

$$F_{\max} = \sqrt{(2 \cdot \mathrm{TIE} \cdot K)} \tag{2}$$

The initial stiffness measured from the force-deflection graphs was used for K in the equations.

Figs 8–10 summarise the results of the damage analyses. Fig. 8 shows the lower CFM crack length and average vertical matrix crack spacing in the UD layer versus TIE. For clarity, the error bars are not shown for the matrix crack spacing because the variation was very wide and there was no visible trend in the results (this was true for all these coupon configurations). It was

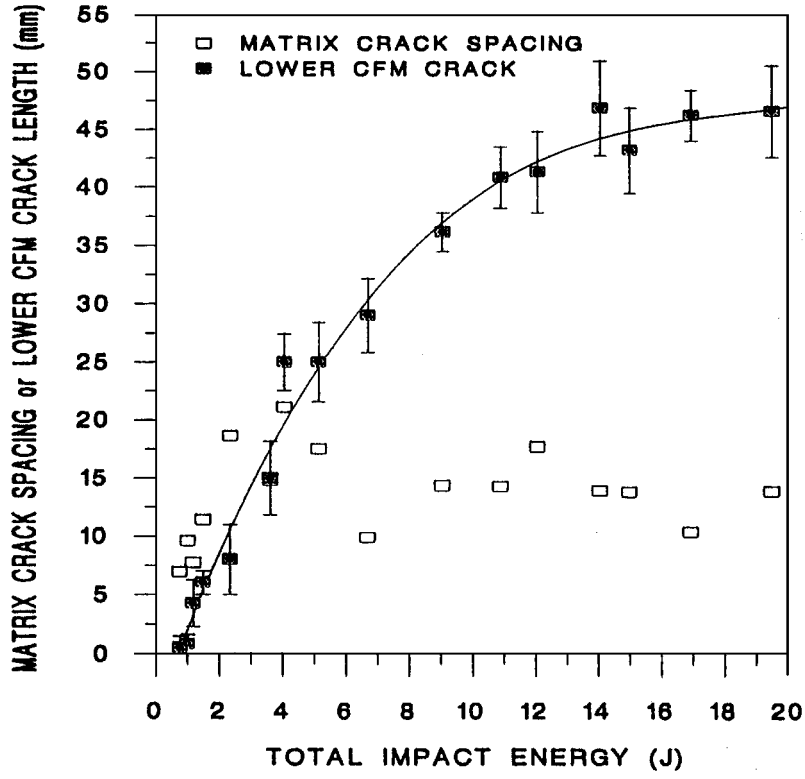

Figure 8 Lower CFM crack length and UD matrix crack spacing versus for the shear coupon.

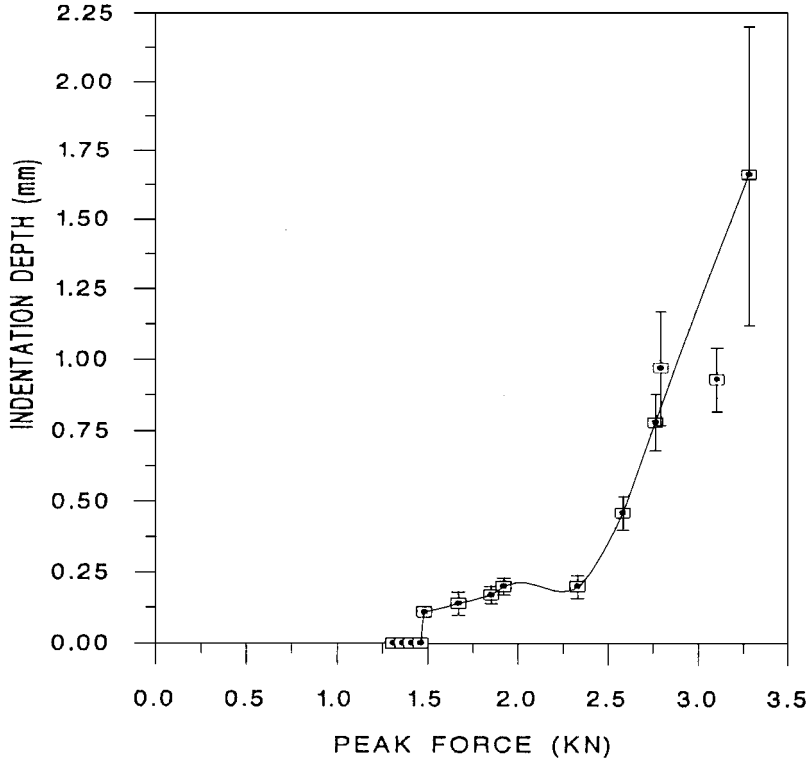

Figure 9 Indentation depth versus peak force for the shear coupon.

concluded that the lowest energy impacts performed were still above the onset of matrix cracking and that over the energy range tested the matrix crack density did not increase.

The lower CFM crack grew longitudinally as the coupon was less stiff in the transverse direction. The rate of lower CFM crack growth (Fig. 8) was constant up to approximately 25 mm length, but then the growth rate decreased and levelled off at approximately 45 mm, due to the clamped supports (60 mm internal diameter). The onset of lower CFM cracking occurred at 1.3 kN, which coincides with the "knee" on the force-deflection curve.

Due to the clamped supports the shear coupon was relatively stiff and therefore the permanent indentation could not be ignored as a damage energy absorbing

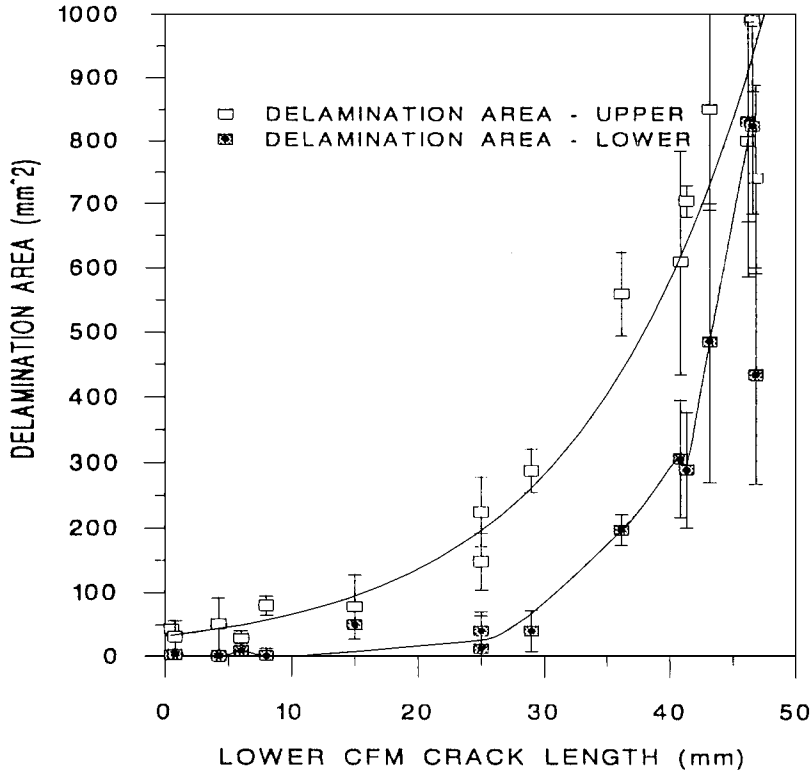

Figure 10 Delamination areas versus lower CFM crack length for the shear coupon.

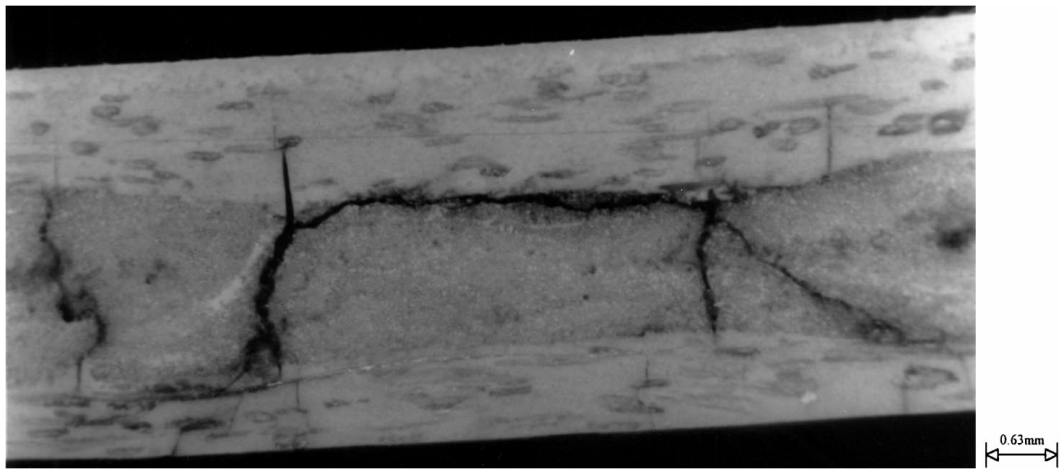

Figure 11 Photograph of upper interface delamination and associated shear/tensile UD matrix cracks of a 1.02 J TIE shear coupon.

mode. Fig. 9 illustrates that permanent deformation of the impacted surface initially occurred at approximately 1.5 kN, from which point the indentation deepened, as the peak force increased. The jump in indentation depth above 2.4 kN corresponded to the first sign of shear cracking on the upper CFM surface directly under the edge of the impactor (confirmed by thermal deply analysis which identified CFM fibre breakage under the impactor for these coupons). The large error bar for the final point indicates that the penetration threshold was being approached. The initial indentation was observed as stress-whitening (matrix cracking and surface microbuckling) as described by Zhou and Davies [14] who also observed ply "shear-out" which corresponds to the shear cracking of the impacted ply.

Delamination areas calculated from optical microscopy (Fig. 10) and C-scan were favourably compared, but as the optical microscopy results gave both an upper and lower interface area/pattern as compared to the plan view of the damage by C-scan, only the former are included in this paper. The delamination of the upper interface occurred at the lowest energy tested which generated a peak force of 1.3 kN and was therefore another damage mode contributing to the "knee". Shear cracks and/or vertical tensile cracks in the UD ply were almost always found at the edges of the upper interface delamination (Fig. 11).

The upper interface delamination grew longitudinally (Fig. 12) spreading to a width of approximately 10 mm corresponding to the impactor diameter and the "generator strip" referred to by Malvern *et al.* [23]. From their impact tests on cross-ply glass/epoxy with a blunt ended impactor, they reported a delamination, of width corresponding to the impactor diameter, bounded

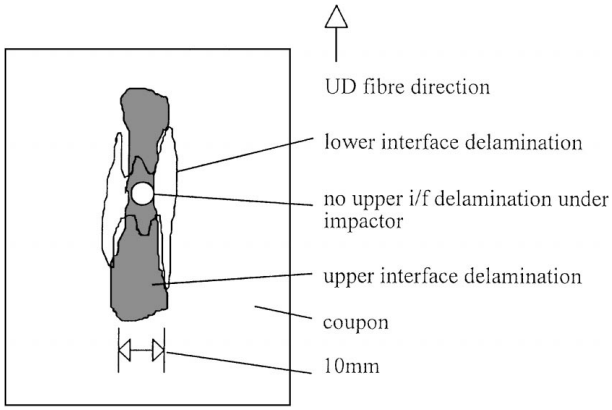

Figure 12 Upper and lower interface delamination patterns in the shear coupon.

by two through thickness shear cracks. The "generator strip" lengthened parallel to the fibres as result of the upper layer being forced through the laminate by the impactor.

The growth in delamination corresponds to the softer section of the force-displacement graph (Fig. 6) above the "knee", correlating well with the findings of Zhou and Davies [14]. Upper interface delamination was in general not found directly under the impactor due to the high compressive normal forces generated, but much shear cracking in the UD layer was present due to the high contact forces.

The upper interface delamination was initiated by the high shear stresses induced by the clamped supports and by a transverse UD matrix crack (Fig. 13a). The growth was relatively linear with both TIE and peak force but less so with lower CFM crack length (Fig. 10). The lower CFM crack assisted delamination growth because it propagated through to the UD layer in the form of a longitudinal UD matrix crack, increasing the Mode I energy available for opening the upper interface delamination (Fig. 14). Fig. 10 suggests that above a lower CFM crack length of 25 mm, the rate of upper interface delamination increased, due to this effect.

Two separate forms of lower interface delamination were observed which merged at higher energies. Firstly, **shear induced lower interface delamination** initiated from the 45° UD shear cracks dropping down from the upper interface delamination as shown in Figs 13a and 14. This type of delamination formed outside the upper interface delamination (Fig. 12). Up to 4 J TIE all the observed lower interface delamination was induced by this mechanism. Secondly, **bending induced lower interface delamination** originated under the impactor due to the lower CFM crack (Fig. 13b). As this form of lower interface delamination developed, it grew as an oval with its long axis in the UD fibre direction as illustrated in Fig. 12. AT 4 J TIE the bending induced lower interface delamination was first observed by optical microscopy, and was seen to follow the lower CFM crack. The lower CFM crack formed due to transverse bending, and the delamination due to longitudinal bending as both occur under the circular support conditions. At a lower CFM crack length of 25 mm lower interface delamination growth increased rapidly in parallel with the upper interface delamination (Fig. 10).

As the TIE increased, the number of shear cracks in the UD layer under the impactor increased. When allied to the crushing caused by the compressive forces this resulted in considerable UD fibre-matrix debond. As the support from the UD layer reduced, the upper CFM layer collapsed under the impactor leading to complete penetration. The area of UD fibre-matrix debond increased up to penetration by spreading away from the impact site under the upper interface delamination, and was therefore a large mode of damage energy absorption at high TIE. In the penetrated specimens, the UD fibre breakage extended to a width corresponding approximately to the diameter of the impactor.

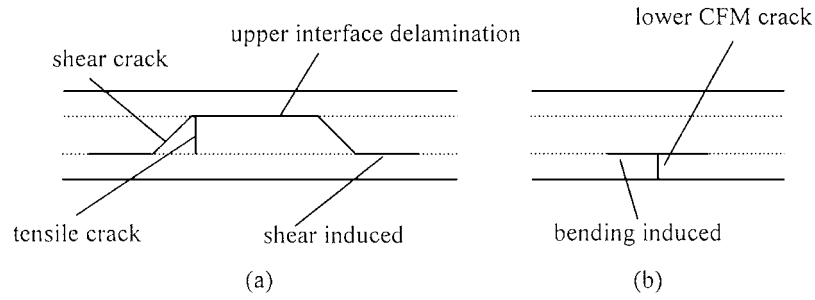

Figure 13 Types of delamination in the shear coupon.

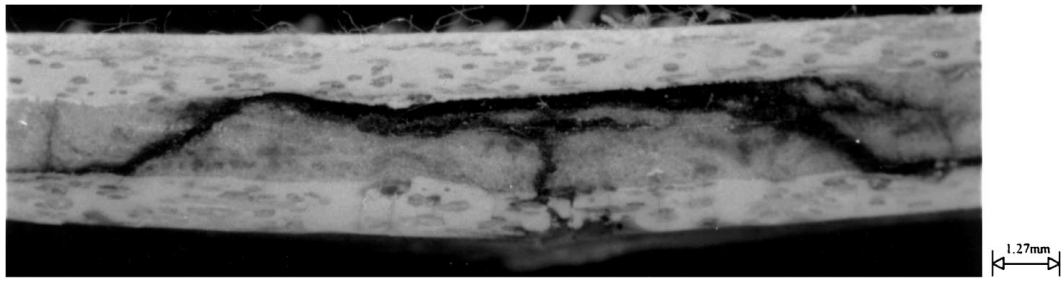

Figure 14 Photograph of lower interface delamination induced by 45° UD shear cracks in the 14 J TIE shear coupon.

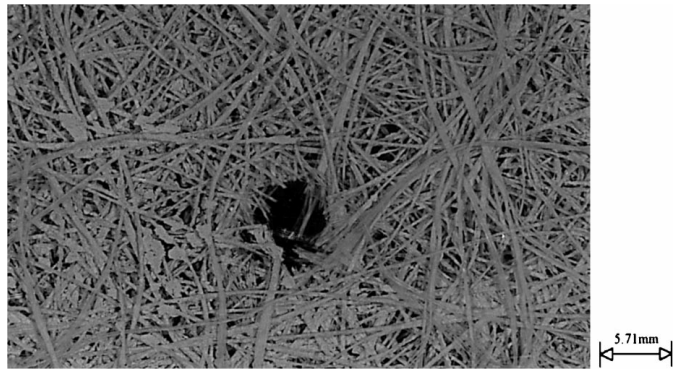

Figure 15 Photograph of fibre breakage under the impactor in the upper CFM layer above 9 J TIE for the shear coupon from thermal deply exercise.

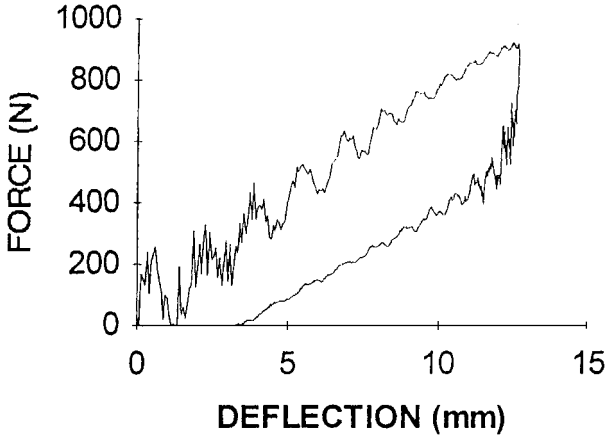

Figure 16 Force-deflection curve for the 6.4 J TIE transverse coupons (Figure 4.8).

Only a very small amount of fibre breakage in the UD layer was found in unpenetrated coupons, where it was limited to the lower tensile surface of the UD layer (see Fig. 15).

3.2. Transverse coupon

It is clear from Fig. 16 showing a typical force-deflection curve at 6.4 J TIE, that the vibration response on top of the curve was quite prominent making it difficult to interpret damage initiation directly. In contrast to the shear coupon, the majority of damage occurred at peak force when there was a large load drop, therefore the damage can be termed unstable. This coupon was less stiff than the shear coupon due to the geometry and supports, and because there was no UD fibres in the major plane of bending. The peak forces generated were therefore much lower than reported above.

Fig. 17 displays good correlation between the experimental results and the peak force predicted by the modified spring-mass model for the first three points. At higher energies the curve deviated from an elastic response and final failure occurred in the form of "creasing" and not penetration for the two highest energy tests in this series. "Creasing" occurred when the lower CFM crack had traversed the width of the specimen

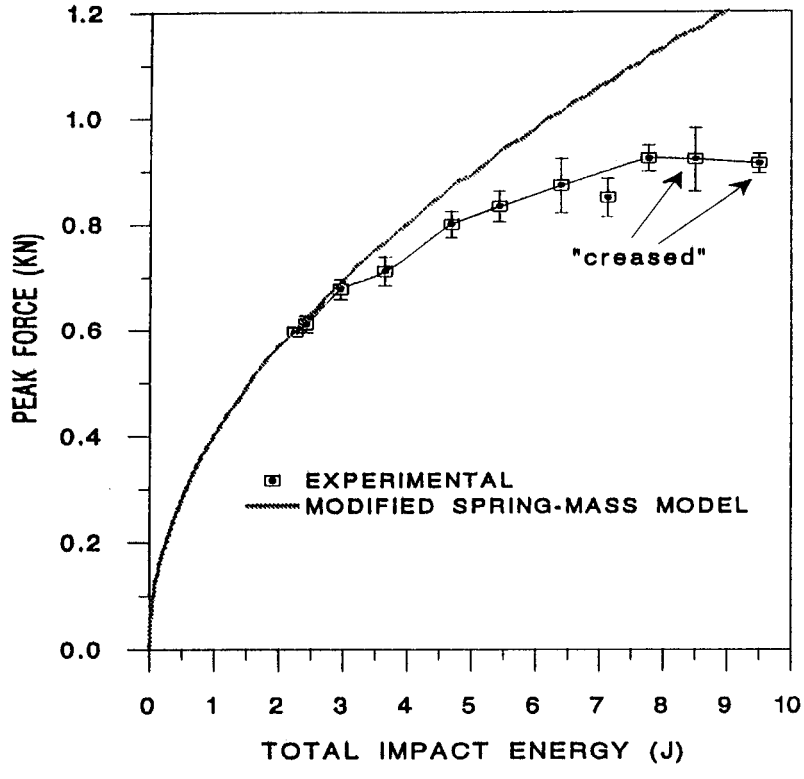

Figure 17 Peak force versus TIE for the transverse coupon, and modified spring-mass model prediction.

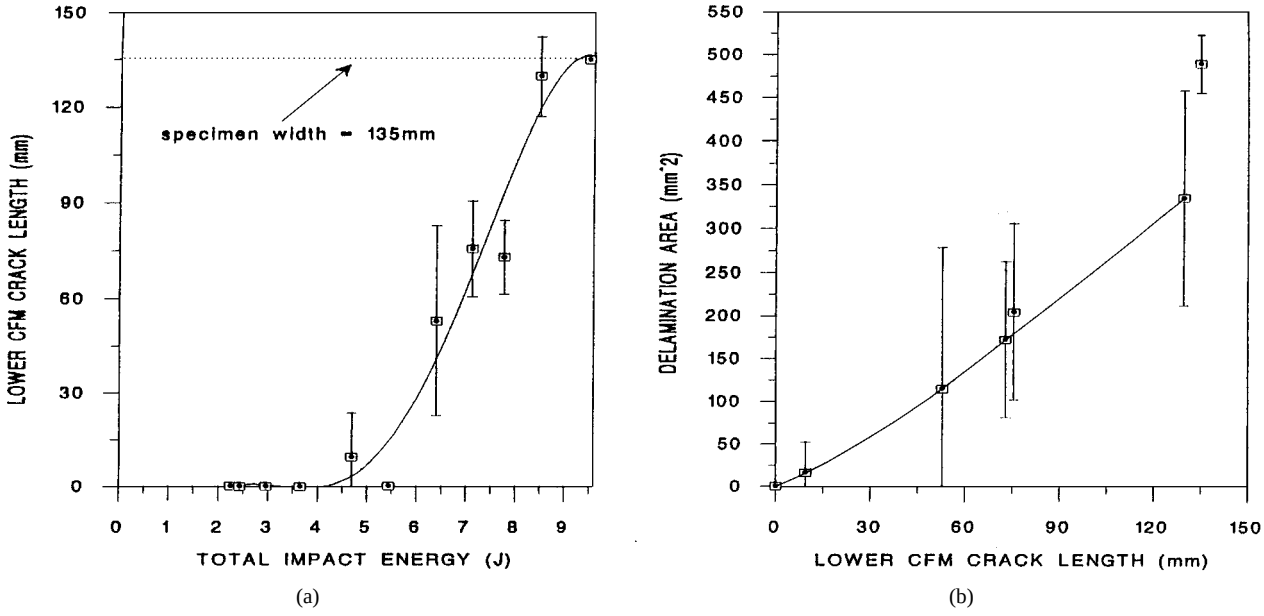

Figure 18 Lower CFM crack length versus TIE (a) and delamination area versus lower CFM crack length (b) for the transverse coupon.

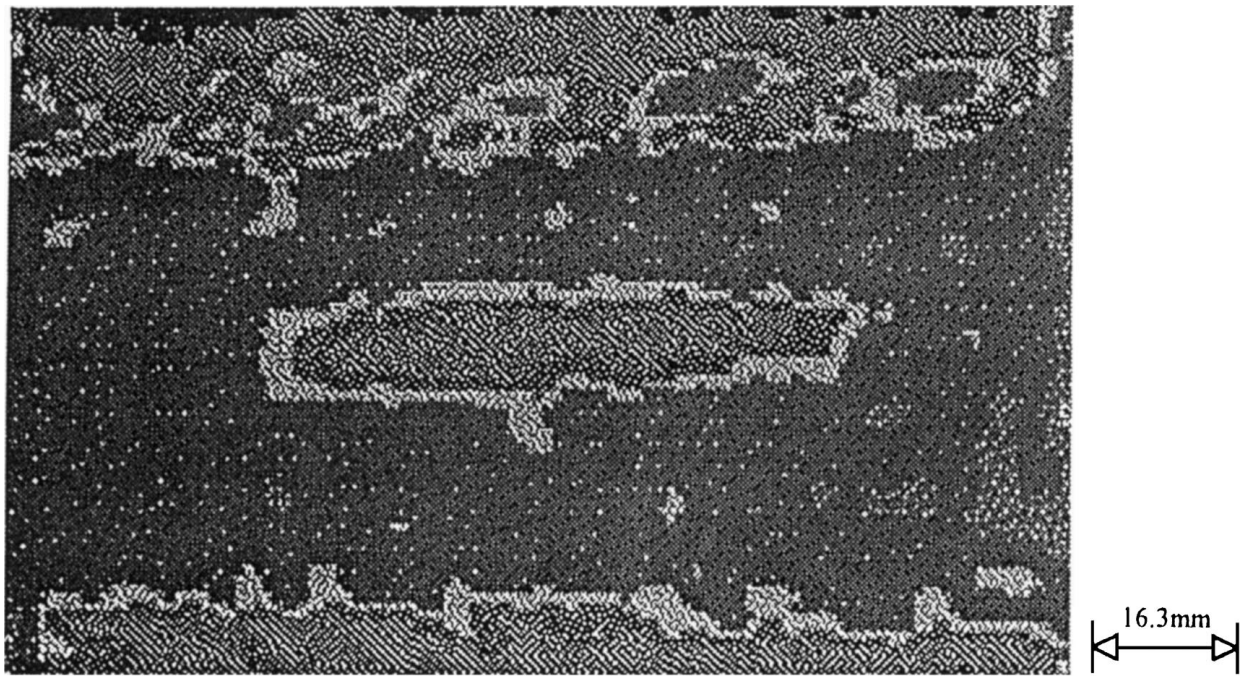

Figure 19 C-scan plot from a 8 J TIE transverse coupon (the attenuation along the edges are due to the tapers/webs and not damage).

which then folded along the crack because only the upper CFM had any remaining strength.

Due to the simple supports and there being only one plane of bending, the damage analysis was less complex than in the previous section. The damage response was dominated by the lower CFM crack and associated upper interface delamination and the damage analysis very clearly explained the impact test data. Fig. 18a shows the lower CFM crack length versus TIE and illustrates that the crack was initiated between 4.5 and 5.5 J. The graph also illustrates that once lower CFM cracking began, growth was rapid (and therefore less stable and less repeatable hence the jumps in the curve) corresponding to the unstable nature of the load drop in Fig. 16. At the highest crack length the specimen width limited crack growth.

Fig. 18b indicates the linear relationship between lower CFM crack length and upper interface delamination area, except for the final point where the CFM crack had reached the edge of the specimen. This relationship arises because the CFM crack propagates straight through the UD layer and as the crack reaches the upper interface, it is redirected into a delamination. Upper interface delamination was initiated as soon as a lower CFM crack occurred and it was these two forms of damage which caused the flattening of the peak force curve in Fig. 17. The delamination extended along the length of the crack but remained thin as illustrated by the C-scan in Fig. 19.

Specimens from the two highest energy sets of tests were tested for fibre breakage using the thermal deply technique and no fibre failure was found in the UD layer

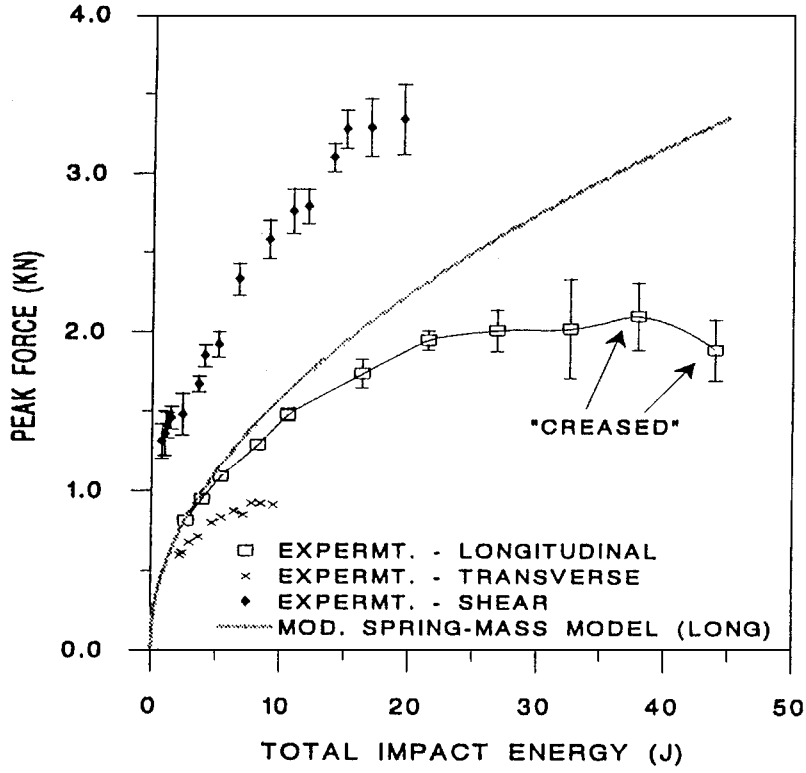

Figure 20 Peak force versus TIE for the longitudinal coupon, and modified spring-mass model predictions, in comparison with the shear and transverse coupon experimental results versus TIE.

or upper CFM layer. This is because upper CFM damage directly under the impactor is governed by the peak force, which in this case was quite low, and certainly below the 1.5 kN force at which permanent indentation was first observed for the shear coupon tests. Throughout the energy range there was no shear cracking in the UD layer, which was due to the simple supports inducing bending rather than shear forces.

3.3. Longitudinal coupon

The force-deflection response for this coupon was very similar to the transverse coupon with damage occurring at peak force in the same way as the transverse coupon but with a stiffer response. Fig. 20, containing all three coupon configuration test results, shows that the peak force rose in agreement with the predicted elastic response curve to approximately 5 J and then the gradient gradually reduced up to 21 J, above which the peak force flattened off at 2.0 kN. Final failure occurred in a "creasing" mode for the two highest energies tested, as a consequence of the lower CFM crack extending across the width of the specimen.

The various forms of lower surface cracking in Fig. 21 were the first signs of visible damage and were complex due to the tapers on the lower surface:

Lower CFM crack: transverse tensile crack formed under the impactor.

Taper crack: a transverse tensile crack through the wrap-around ply forming the taper.

Taper-line crack: a longitudinal tensile crack caused by the ply-drop-off at the end of the wrap-around ply, running along the taper-line.

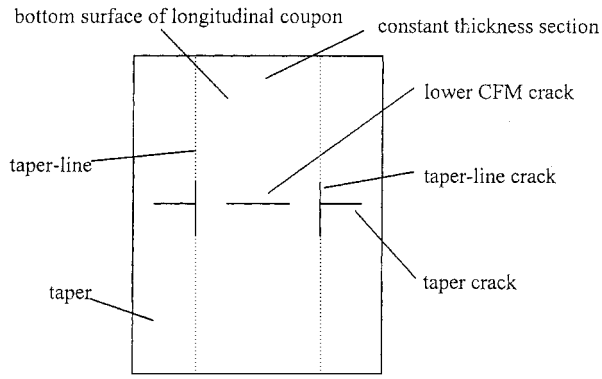

Figure 21 Cracking on the lower surface of the longitudinal coupon.

The lower CFM crack was initiated at approximately 5 J and grew quite linearly with TIE, which corresponds to the reduction in stiffness response from 5 J in Fig. 20. The taper crack and taper-line crack were initiated between the 16 and 21 J TIE sets of tests. It is these forms of cracking and associated delamination which were a prime cause of the reduction in stiffness response above 21 J.

Fig. 22a shows the delamination areas plotted against TIE, with rapid delamination growth above 27J TIE, which corresponds to the flattening off in the peak force above this energy.

The most significant forms of delamination were at the lower interface (delamination – lower (central)) and along the interface between lower CFM and wrap-around ply (delamination – lower (side)). The delamination – lower (side) could also be considered to be a "debond" of the web from the skin. The lower CFM crack initiated the lower interface

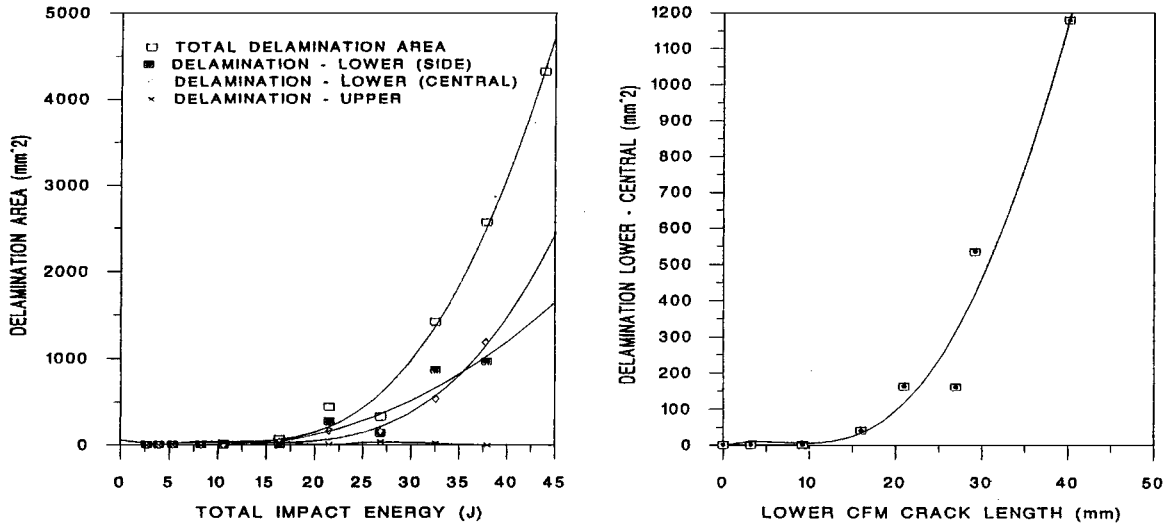

(a) (b)

Figure 22 Delamination areas versus TIE (a) and lower interface delamination (central) versus lower CFM crack length for the longitudinal coupon (b).

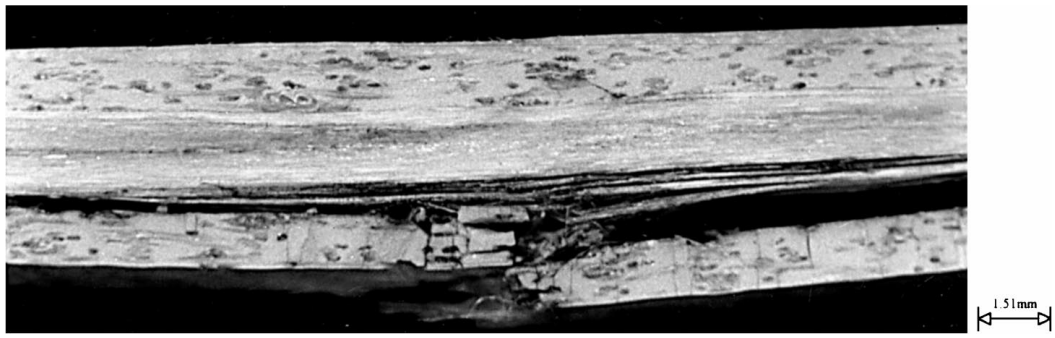

Figure 23 Photograph of lower interface delamination initiated by a lower CFM crack and UD fibre failure in a 44 J TIE longitudinal coupon.

delamination – (central) because when the crack reached the lower interface it was redirected by the longitudinal fibres in the UD layer into a delamination (Fig. 23). Fig. 22b shows the relationship between the lower CFM crack and lower interface delamination (central) and suggests an initiation crack length of 10 mm above which delamination growth increased rapidly. Fig. 22a indicates that there was some upper interface delamination but this remained very small, and was due to the high shear stresses local to the impactor, as this form of delamination was only found adjacent to the impact site.

Under the impactor, upper CFM damage consisted initially of permanent indentation and then shear cracking. An indentation was just visible at 8 J TIE (1.3 kN – as compared to 1.5 kN for the shear tests) and increased to approximately 0.15 mm before shear cracking occurred at 32 J (2 kN). "Creasing" failure occurred before the shear cracks had passed through the upper CFM layer.

Considerable UD fibre breakage occurred before final failure. As the lower surface CFM crack grew, the stresses in the UD layer increased dramatically especially in the lowermost fibres, producing UD fibre breakage prior to final failure (Fig. 23).

There were a large number of damage modes for this impact configuration, due to the tapers on the lower surface. The interactions in the higher energy tests could not be described sufficiently due to their complexity. However, the initial onset of central lower CFM cracking and associated delamination was clearly identified and correlated with the change in stiffness response in Fig. 20.

4. Conclusions

The coupon tests have thus provided a great deal of information regarding the behaviour of the basic pultruded composite in shear, and transverse and longitudinal bending:

1. Lower CFM cracking was critical as it directly initiated lower interface delamination under longitudinal bending and indirectly initiated, via transverse UD matrix cracking, upper interface delamination under transverse bending. Under shear loading upper interface delamination was induced by high shear forces and a transverse UD matrix crack prior to promotion via a lower CFM crack. Thus for this lay-up the lower CFM crack can be likened to the critical matrix crack referred to by Chang and co-workers [24] which initiated delamination in 0/90 laminates.

2. UD shear cracking also occurred, which under shear loading only initiated lower interface

delamination. Shear cracks in the UD layer initiated lower interface delamination, as reported by Joshi and Sun [25] for 0/90 lay-ups. Thus, delamination only occurred in the presence of an initiating crack as was first reported by Takeda [26].

3. Transverse UD matrix cracking occurred at energy levels below that tested, whilst only limited UD fibre breakage was observed prior to final failure.

4. When very high contact forces were induced (e.g. in the shear coupon), and the indentation under the impactor reached a critical level, the upper CFM cracked through. This form of upper CFM failure was labelled ply "shear-out" by Zhou and Davies [14] in their impact work on thick glass/polyester laminates. For the shear coupon at high energy levels UD shear cracking was so dense under the impactor that considerable fibre-matrix debond occurred in the UD layer.

Prior to this research, the literature contained no detailed impact response and damage analysis regarding a pultruded lay-up. This work has reported in detail the low velocity impact damage modes and interactions for a typical pultruded lay-up – one unidirectional fibre (UD) layer sandwiched between two continuous filament mats (CFM). From each of the coupon tests the damage observed and the reduced stiffness response of the force-deflection curves were closely correlated. Interlaminar damage (delamination) was always initiated by some form of intralaminar damage (lower CFM cracking, vertical tensile matrix cracks and/or inclined shear cracks).

Acknowledgements

We would like to thank our colleagues at Maunsell Structural Plastics, European Intermodal Products, Rosand, Pera International and within Loughborough University for all their invaluable support during this research.

References

1. S. ABRATE, *Appl. Mech. Rev.* **44** (4) (1991) 155–190.
2. G. CAPRINO, *J. Compos. Mater.* **18** (1984) 508–518.
3. H-Y. T. WU and G. S. SPRINGER *ibid.* **22** (1988) 533–560.
4. A. T. NETTLES and A. J. HODGE, Twenty Third International SAMPE Technical Conference, Covina, USA, October 1991, pp. 177–183.
5. R. JONES, J. PAUL, T. E. TAY and J. F. WILLIAMS, *Compos. Struct.* **10**(1) (1988) 51–73.
6. M. O. W. RICHARDSON and M. J. WISHEART, *Composites* **27** (1996) 1123–1131.
7. N. SELA and O. ISHAI, *ibid.* **20**(5) (1989) 423–435.
8. S. R. FINN, Y-F. HE and G. S. SPRINGER, *Compos. Struct.* **23** (1993) 191–204.
9. H. Y. CHOI, R. J. DOWNS and F-K. CHANG, *J. Compos. Mater.* **25** (1991) 992–1011.
10. M. J. WISHEART, Impact properties and finite element analysis of a pultruded composite system, PhD thesis, Institute of Polymer Technology and Materials Engineering, Loughborough University, 1996.
11. M. J. WISHEART and M. O. W. RICHARDSON, Analysis of strain-rate effects on the low velocity impact response of a pultruded glass/polyester composite, submitted.
12. A. L. SVENSON, M. W. HARGRAVE and L. C. BANK, *Eng. Plas.* **7**(3) (1994) 173–186.
13. S. S. HABIB, *Journal of Reinforced Plas. Compos.* **14**(8) (1995) 799–803.
14. G. ZHOU and G. A. O. DAVIES, *Int. J. Impact Eng.* **16**(3) (1995) 357–374.
15. T. C. LINDSAY and D. J. WILKINS, Twenty Third International SAMPE Technical Conference, Covina, USA, October 1991, pp. 72–90.
16. A. E. JOHNSON, D. R. MOORE, R. S. PREDIGER, P. E. REED and S. TURNER, *J. Mater. Sci.* **21** (1986) 3153–3161.
17. S. L. KESSLER, G. C. ADAMS, S. B. DRISCOLL, and D. R. IRELAND, Instrumented impact testing of plastics and composite materials, ASTM STP 936 (American Society for Testing and Materials, Philadelphia, 1987).
18. R. A. CHIVERS and D. R. MOORE, *Measurement Sci. Technol.* **1** (1990) 313–321.
19. D. P. JONES, D. C. LEACH and D. R. MOORE, *Plastics and Rubber Processing and Applications* **6**(1) (1986) 67–79.
20. D. R. MOORE and R. S. PREDIGER, *Polym. Compos.* **9**(5) (1988) 330–336.
21. S. HONG and D. LIU, *Experimental Mechanics* **29** (1989) 115–120
22. W. C. JACKSON and C. C. POE, Jr., *J. Compos. Technol. Res.* **15**(4) (1993) 282–289.
23. L. E. MALVERN, R. L. SIERAKOWSKI and C. A. ROSS, "Impact failure mechanisms in fiber-reinforced composite plates," High Velocity Deformation of Solids Conference, August 1977, (Tokyo, 1978) pp. 120–131.
24. F-K. CHANG, H. Y. CHOI and S-T. JENG, *Mech. Mater.* **10** (1990) 83–95.
25. S. P. JOSHI and C. T. SUN, *Journal of Composite Materials* **19** (1985) 51–66.
26. N. TAKEDA, R. L. SIERAKOWSKI and L. E. MALVERN, *Compos. Technol. Rev.* **4**(2) (1982) 40– 44.

Received 1 March 1997
and accepted 18 August 1998